EPJ A direct
electronic only

Indirect measurement of the ^{15}N(p, α)^{12}C reaction cross section through the Trojan-Horse Method

M. La Cognata[1,2], S. Romano[1,2], C. Spitaleri[1,2,a], R. Tribble[3], L. Trache[3], S. Cherubini[1,2], Changbo Fu[3], L. Lamia[1,2], A. Mukhamedzhanov[3], R.G. Pizzone[1,2], C. Rolfs[4], G. Tabacaru[3], and A. Tumino[1,2]

[1] Dipartimento di Metodologie Fisiche e Chimiche per l'Ingegneria - Università di Catania, Catania, Italy
[2] Laboratori Nazionali del Sud - INFN, Catania, Italy
[3] Cyclotron Institute, Texas A&M University, College Station, TX, USA
[4] Ruhr-Universität, Bochum, Germany

Abstract. The low-energy, bare-nucleus cross section for ^{15}N(p, α)^{12}C is extracted by means of the Trojan-Horse Method applied to the ^{2}H(^{15}N, α^{12}C)n reaction at $E_{beam} = 60$ MeV. The astrophysical S-factor is compared to the direct data in the same energy region. A nice agreement shows up down to 100 keV, while the low-energy behaviour of the S-factor suggests a smaller rate than is reported in the literature.

PACS. 24.10.-i Nuclear Reaction Models and Methods – 26.20.+f Hydrostatic Stellar Nucleosynthesis

1 Introduction

The importance of ^{19}F in astrophysics is two-fold: in red giants fluorine is enhanced by large factors with respect to the solar abundance; on the other hand, the fluorine abundances observed in giants can constrain AGB star models [1]. Primary sources of uncertainty in predicting fluorine abundances in AGB stars come from the adopted reaction rates and the treatment of nucleosynthesis during the thermal pulses and the interpulse periods [2].

The reaction rate for the ^{15}N(p, α)^{12}C affects the production of fluorine since it removes both protons and ^{15}N nuclei from the ^{19}F production chain [1]. Calculations show that even the highest experimentally observed surface fluorine abundances are reproduced for some masses and metallicities, but this occurs for C/O values much larger than what experimental data suggest [1]. In fact ^{12}C and ^{19}F are correlated since they are both dredged up to the stellar surface in correspondence of the third dredge-up. The ^{15}N(p, α)^{12}C reaction rate introduces at least an 8% uncertainty in the fluorine surface abundance [1], since NACRE [3] and CF88 [4] rates show up a factor 2 difference.

As the ^{15}N(p, α)^{12}C experimental cross section is measured down to 80 keV [5], much larger than the Gamow peak energy (8 keV), only extrapolations are available in the low energy region.

1.1 The Trojan-Horse Method

The measurement of nuclear cross sections at ultra-low energies is a very difficult task because of the presence of the Coulomb barrier exponentially damping the cross section. Therefore extrapolation is necessary when data at astrophysical energies are unavailable, thus introducing additional uncertainties related to poorly known low-energy or subthreshold resonances and to the electron screening effect [6]. The extrapolation procedure is usually performed on the astrophysical factor

$$S(E) = E \cdot \exp(2\pi\eta) \cdot \sigma(E), \qquad (1)$$

where η is the Sommerfeld parameter, $S(E)$ being a smoothly varying function of the energy even in the sub-Coulomb region. A possible way to avoid extrapolation from data at energies much higher than the Gamow window is the application of the Trojan-Horse Method.

The Trojan-Horse Method (THM) [7,8] is an indirect method that allows for the extraction of the bare nucleus cross section of a two-body reaction of astrophysical interest,

$$A + x \rightarrow c + C, \qquad (2)$$

by selecting the Quasi-Free (QF) contribution of the cross section of a suitable three-body process

$$A + a \rightarrow c + C + s, \qquad (3)$$
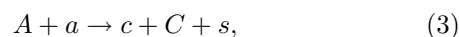
where x acts as participant and s as a spectator to the two-body reaction. If the energy of the projectile A is higher

than the Coulomb barrier in the $A + a$ channel, then the reaction (2) can be induced inside the nuclear interaction field. The nucleus a, having a high probability for the $x \oplus s$ configuration, constitutes the so-called *Trojan-Horse Nucleus* since it brings the cluster x inside the target A nuclear field. Therefore the Coulomb barrier and electron screening effect are negligible and a measurement of the cross section at ultra-low energies is possible.

In the simple Plane-Wave Impulse Approximation (PWIA) post-form approach [8] the two-body bare nucleus cross section is extracted from the measured three-body cross section using the equation

$$\frac{\mathrm{d}^3\sigma}{\mathrm{d}E_C\mathrm{d}\Omega_C\mathrm{d}\Omega_c} \propto KF\,|G(p_s)|^2\,\frac{\mathrm{d}\sigma_l^N}{\mathrm{d}\Omega}\,, \qquad (4)$$

where KF is a kinematical factor, $|G(p_s)|^2$ the momentum distribution of spectator particle s inside a and $\mathrm{d}\sigma_l^N/\mathrm{d}\Omega$ the *nuclear* (off-energy-shell) cross section, under the hypothesis of a dominant l-contribution. In fact, since the reaction (2) is induced inside the short-range nuclear field the penetration probability of the Coulomb barrier has to be introduced in order to compare the THM cross section with the direct data from literature in the energy region below the Coulomb barrier [9]:

$$P_l(k_{Ax}R) = \frac{1}{F_l^2(k_{Ax}R) + G_l^2(k_{Ax}R)}\,, \qquad (5)$$

where F_l and G_l are the regular and irregular Coulomb wave functions, k_{Ax} and R the $A-x$ relative wave number and interaction radius, respectively.

In the present work, the measurement of the bare-nucleus cross section for the $^{15}\mathrm{N}(\mathrm{p},\alpha)^{12}\mathrm{C}$ reaction is presented in the astrophysically relevant energy region, from $600\,\mathrm{keV}$ down to $5\,\mathrm{keV}$. The indirect two-body cross section is extracted in arbitrary units from the $^2\mathrm{H}(^{15}\mathrm{N},\alpha\,^{12}\mathrm{C})\mathrm{n}$ coincidence yield in the PWIA approach and is normalized to the direct data to get the absolute cross section. In the measured energy region, the $^{15}\mathrm{N}(\mathrm{p},\alpha)^{12}\mathrm{C}$ cross section is dominated by the 1^- resonance at $314\,\mathrm{keV}$ [3], therefore this study allows one to perform a complete validity test of the THM below the Coulomb barrier.

2 The experiment

The experiment was performed at the Texas A&M University Cyclotron Institute. The K500 superconducting cyclotron provided a $60\,\mathrm{MeV}$ $^{15}\mathrm{N}$ beam with a spot size on target of $1\,\mathrm{mm}$ and intensities up to $5\,\mathrm{nA}$, impinging on a $200\,\mu\mathrm{g/cm}^2$ thick CD_2 target. A simple experimental setup was used: a telescope (A) made up of an ionization chamber and a silicon position-sensitive detector (PSD) to discriminate carbon nuclei, and a couple of silicon PSD's (B, C) on the opposite side with respect to the beam direction. Two kinds of event were recorded: coincidences between A and B or between A and C. The angular condition were selected in order to maximize the quasi-free

Table 1. Laboratory central angles (θ_0), angular range spanned $(\Delta\theta)$, solid angle subtended $(\Delta\Omega)$ and thickness (d) for each detector.

Detector	θ_0 (deg)	$\Delta\theta$ (deg)	$\Delta\Omega$ (msr)	d (mm)
ΔE-A	15.0	–	–	50
PSD-A	15.0	11.1	8.7	0.492
PSD-B	12.2	13.1	11.2	0.984
PSD-C	32.2	16.7	20.0	0.984
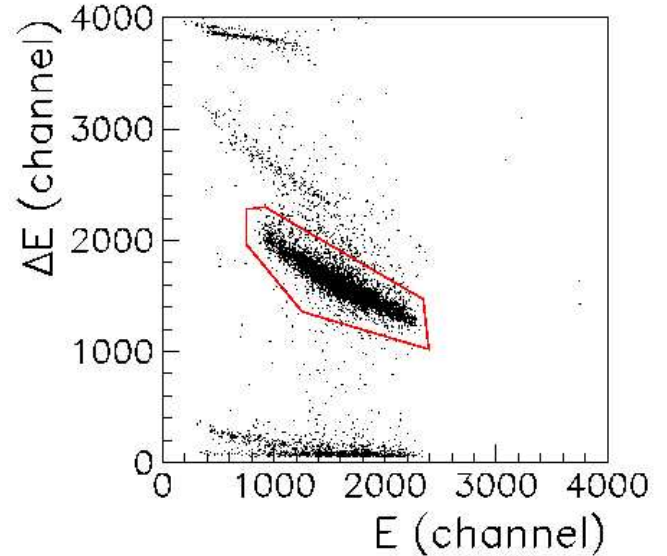
Fig. 1. Typical ΔE-E spectrum for the A telescope. The graphical selection shown in the picture marks the locus of carbon nuclei.

contribution: table 1 shows the laboratory angles for all the coincidence detectors.

The ionization chamber was filled with $60\,\mathrm{mbar}$ butane and was closed on both side by $1.5\,\mu\mathrm{m}$ thick Mylar foil windows; overall energy resolution turned out to be about 15%, therefore one could not discriminate $^{12}\mathrm{C}$ nuclei from $^{13}\mathrm{C}$ and an off-line kinematical selection was required. A typical ΔE-E spectrum is shown in fig. 1. The carbon locus is selected by means of a graphical cut as shown in the figure. The alpha-particle discrimination is obtained by selecting the kinematical locus of the three-body reaction.

The spectator particle momentum range spanned in the experiment is such that a comparison of the coincidence yield for small p_s (less than $20\,\mathrm{MeV}/c$) and larger p_s can be performed, in order to check that the resonances occurring in the 2-body reaction are fed through a quasi-free channel and not through sequential decay of intermediate nuclei.

2.1 Data analysis

After detector calibration, the first step of the analysis is the selection of the events corresponding to the three-body reaction $^2\mathrm{H}(^{15}\mathrm{N},\alpha\,^{12}\mathrm{C})\mathrm{n}$. This is accomplished through a
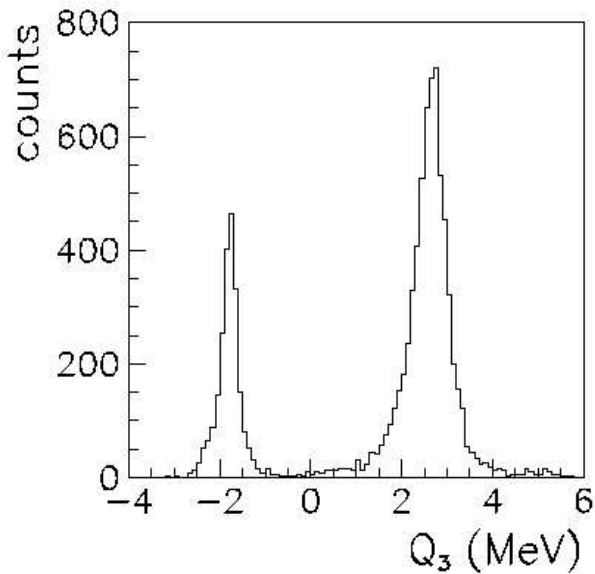
Fig. 2. Three-body Q-value spectrum. Two peaks corresponding to the ground state and first excited state (4.4389 MeV) of ^{12}C are clearly visible.

selection of coincidence events and of the reaction kinematical locus. For the selected events the Q-value is calculated by imposing energy balance for the three-body reaction. In fig. 2 the Q-value spectrum is reported, showing two peaks corresponding to the ground state and first excited state of ^{12}C (Q-values 2.74 MeV and -1.70 MeV respectively).

The good agreement between the experimental and the theoretical Q-values confirms the accuracy of the calibration. In the subsequent analysis only the events corresponding to the high-energy peak are retained in order to extract the ^{15}N(p, α_0)^{12}C cross section. In fact, the ^{15}N(p, α_1)^{12}C reaction is of negligible astrophysical relevance in the context outlined in the introduction, since its cross section is much lower than the ^{15}N(p, α_0)^{12}C one inside the Gamow peak [5]. For this reason in the following sections the 0 will be dropped.

The second step of the THM data analysis is the study of the reaction mechanisms feeding the exit channel. This is a necessary step to disentangle the QF from the sequential decay mechanisms. Such a selection is fulfilled by investigating the correlation between the relative energies ($E_{\alpha\text{-}n}$ *vs.* $E_{^{12}\text{C-}\alpha}$ and $E_{^{12}\text{C-}n}$ *vs.* $E_{^{12}\text{C-}\alpha}$, as shown in figs. 3a and 3b, respectively) of the detected particles and between $E_{^{12}\text{C-}\alpha}$ and the neutron momentum p_s (fig. 4).

In the α-n *vs.* ^{12}C-α (fig. 3a) and ^{12}C-n *vs.* ^{12}C-α (fig. 3b) relative energy two-dimensional plots very clear vertical loci appear, corresponding to excited states of ^{16}O at 12.44 MeV, 13.09 MeV and 13.26 MeV. An additional contribution to the three-body cross section due to the sequential decay of the excited states of ^{13}C at 6.68 MeV, 7.49 MeV, 7.55 MeV, 7.67 MeV (where the last three levels are not resolved) is also visible, corresponding to the horizontal loci in fig. 3b. Such background processes give
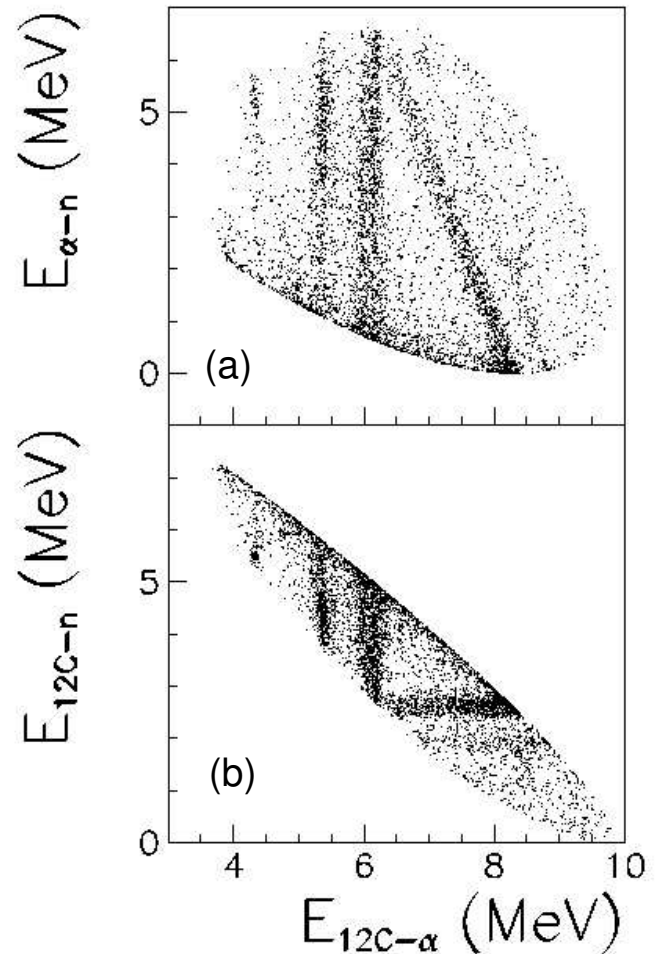
Fig. 3. (a) α-n *vs.* ^{12}C-α and (b) ^{12}C-n *vs.* ^{12}C-α relative energy two-dimensional plot. Very clear vertical loci appear, corresponding to excited states of ^{16}O at 12.44 MeV, 13.09 MeV and 13.26 MeV. The contribution to the three-body cross section due to the sequential decay of the excited states of ^{13}C at 6.68 MeV, 7.49 MeV, 7.55 MeV, 7.67 MeV is also apparent (the horizontal loci in (b)).

a negligible contribution to the coincidence yield in the astrophysical energy region, since in the phase space explored there is no contribution coming from ^{13}C sequential decay at ^{12}C-α relative energies lower than 6 MeV (as it will be shown below zero energy in the ^{15}N(p, α)^{12}C channel corresponds to 4.966 MeV in the ^{12}C-α relative energy).

On the other hand, according to the previous discussion, the occurrence of sequential mechanisms in the ^{12}C-α channel cannot be ruled out by studying the relative energy two-dimensional plots since the same excited state of ^{12}C+α system can be formed through both a quasi-free reaction mechanism and a sequential one. Therefore an investigation of the $E_{^{12}\text{C-}\alpha}$ *vs.* p_s two-dimensional plot is necessary in order to establish the presence of the quasi-free contribution and disentangle the sequential mechanism.
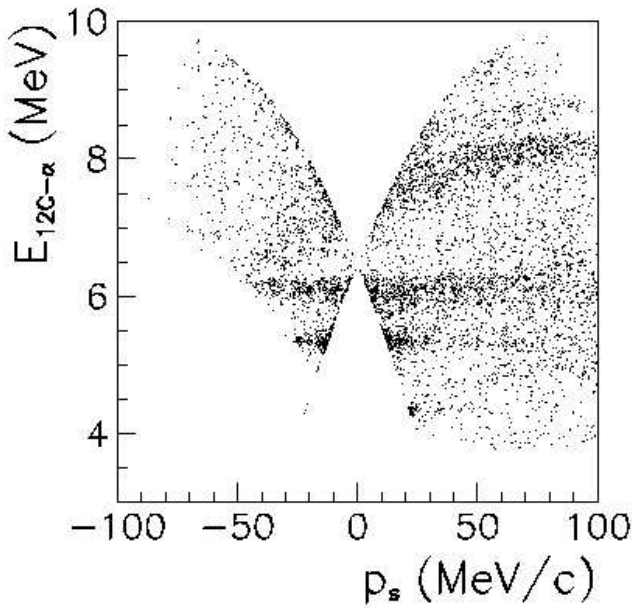
Fig. 4. ^{12}C-α relative energy *vs.* neutron momentum p_s two-dimensional plot. The sharp horizontal lines corresponds to the excited states of ^{16}O at 12.44 MeV, 13.09 MeV and 13.26 MeV. Negligible background coming from ^{13}C sequential decay shows up in the astrophysically relevant energy range.

Figure 4 shows the ^{12}C-α relative energy *vs.* neutron momentum p_s in a two-dimensional plot. The sharp horizontal lines correspond to the excited states of ^{16}O at 12.44 MeV, 13.09 MeV and 13.26 MeV. At higher $E_{^{12}\text{C-}\alpha}$ the occurrence of the ^{13}C sequential decay is clearly visible, but its contribution in the astrophysically relevant energy region is absolutely negligible. From the comparison of the loci corresponding to the different level decays, the quasi-free origin of the ^{16}O levels in fig. 4 is apparent. In fact, while the kinematical locus connected to the ^{13}C decay is still clearly visible at high neutron momentum, the contributions due to the ^{16}O decay is barely visible (in comparison with the background) showing a definite correlation of the coincidence yield for the cited ^{16}O levels with the spectator neutron momentum.

As a further check to determine if the resonances occurring in the ^{12}C-α channel are fed through a quasi free mechanism and not through sequential decay of intermediate nuclei, the $E_{c.m.}$ relative energy for the ^{15}N(p, α)^{12}C reaction, defined as [8]

$$E_{c.m.} = E_{^{12}\text{C-}\alpha} - Q_{2\text{-}body}, \qquad (6)$$

is reported as a function of the momentum p_s of the spectator particle for all coincidence events. In order to explore the behaviour of the coincidence yield as a function of the momentum p_s, the relative energy $E_{c.m.}$ spectra divided by the phase-space contribution were reconstructed for different ranges of the neutron momentum p_s. Within the range 0 to 20 MeV/c (fig. 5, top panel) the coincidence yield appears to be dominated by the decay of the three levels of ^{16}O at 12.44 MeV, 13.09 MeV and 13.26 MeV. For
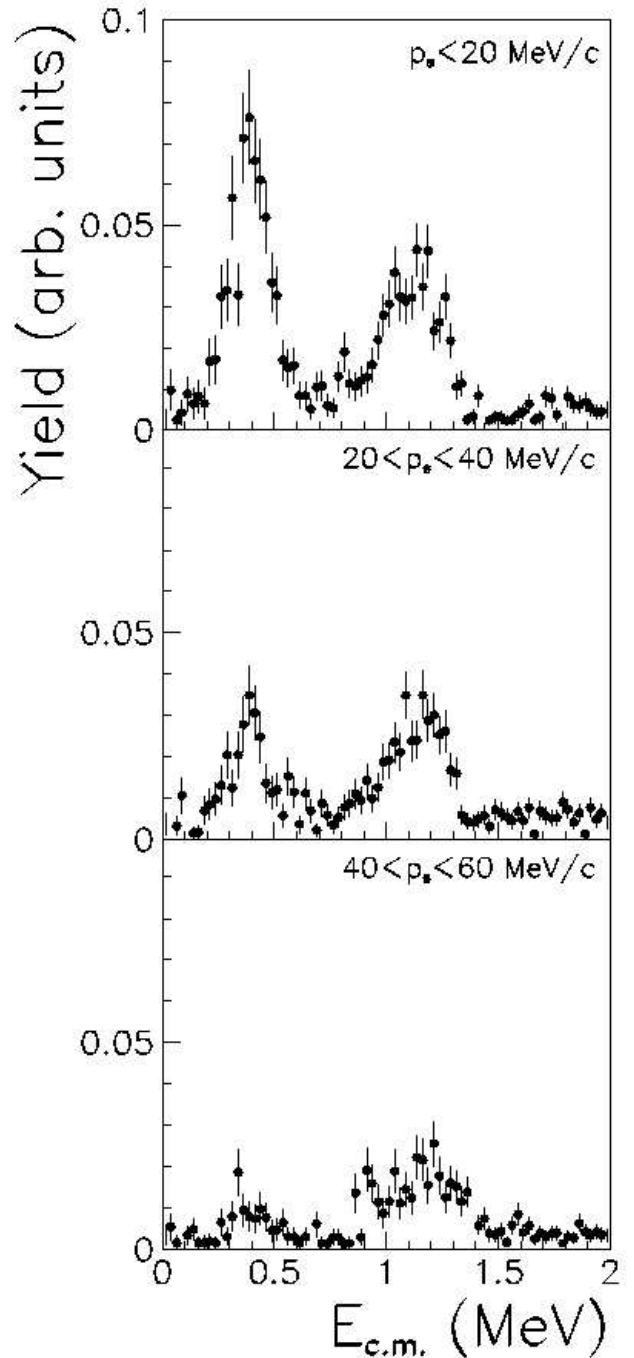

Fig. 5. Correlation spectra between $E_{c.m.}$ and neutron momentum p_s. The excited levels of ^{16}O at 12.44 MeV and 13.09 MeV, 13.26 MeV (not resolved) are clearly visible.

larger p_s, the coincidence yield decreases as shown in fig. 5 (middle panel) and fig. 5 (bottom panel), and such resonances become barely visible with respect to the background. These experimental data provide clear evidence for a strong correlation between coincidence yield and neutron momentum p_s, a necessary condition for the dominance of the quasi-free mechanism in the region approaching zero spectator momentum. In fact this is expected

Table 2. Fitting parameters of the function used to parameterize the bare nucleus THM S-factor, the sum of a 2nd-order polynomial and a Breit Wigner, in which the centroid is fixed at the 1^- resonance energy of 319 keV. In the last column the χ^2 per degree of freedom is also reported.

p_0 (MeVb)	p_1 (MeVb/keV)	p_2 (MeVb/keV^2)	FWHM (keV)	W (MeVb)	χ^2/N
-256 ± 6	-0.82 ± 0.14	$(0.30 \pm 0.03) \cdot 10^{-2}$	190 ± 2	$(0.3193 \pm 0.0016) \cdot 10^8$	2.6
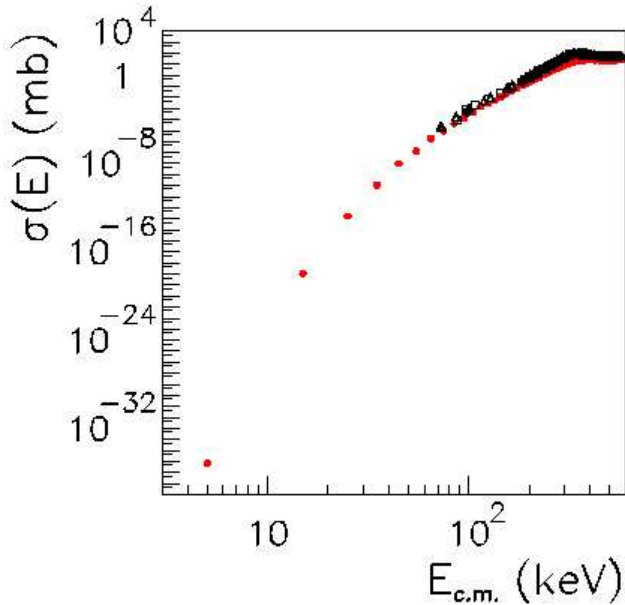
Fig. 6. THM cross section (full dots) together with direct data from [5,10,11] in the energy region between 0 and 600 keV. The lowest energy point correspond to a center-of-mass energy of 5 keV.
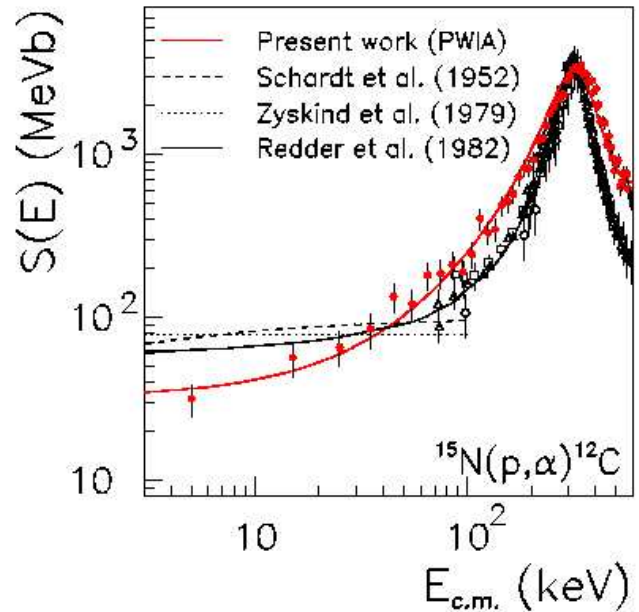

Fig. 7. THM astrophysical $S(E)$ (full red dots) factor together with direct data from [5,10,11] in the low energy region. A fit to the THM bare nucleus S-factor has been performed by means of the sum a Breit-Wigner and a 2nd-order polynomial (parameters in table 2). For comparison, the extrapolation from [5,10, 11] are reported.

3 Results and discussion

Once the quasi-free contribution has been selected, the bare nuclear cross section, $\mathrm{d}\sigma_l^N/\mathrm{d}\Omega$, is extracted by means of eq. (4). A p_s window of 20 MeV/c around zero spectator momentum is adopted in accordance with the previous result.

After penetration probability correction, the THM cross section and astrophysical $S(E)$ factor are extracted and are reported together with direct data [5,10,11] in fig. 6 and in fig. 7: the error bars include only the statistical uncertainties. Here only a minor part of the data is shown, coming from a single pair of detectors (A-C coincidences) and only the simple PWIA approach has been reported: the MPWBA analysis [9,12] is currently in progress.

The THM cross section is normalized to direct data (equating the peak values for the 319 keV resonance) for getting the cross section in absolute units. By fitting $S(E)$ from the indirect data with the sum of a 2nd-order polynomial and a Breit-Wigner (the fit parame-

ters are reported in table 2), $S_{bare}(0)$ is determined to be $S_{bare}(0) = 32 \pm 6$ MeVb (see fig. 7). This is in clear disagreement with direct data extrapolation [5,10,11], giving a much higher value $S_{bare}(0) = 65 \pm 7$ MeVb [5,3]. The present data set also suffers from a systematic error $\sim 20\%$ arising from normalization procedure of the indirect data to the direct ones. The THM $S_{bare}(0)$ value is likely to be an overestimate of the *true* value because of the poorer resolution of THM data with respect to direct measurement, as shown by the larger FWHM of the 319 keV resonance (fig. 7). Such a result tends to reduce the rate for the ^{15}N(p, α)^{12}C in the astrophysically relevant energy region, confirming the value reported in CF88 in contrast with the one cited in NACRE compilation.

The origin of such a disagreement can be traced back to the electron screening effect [6]. In fact the direct data from [5,10,11] were all measured before the middle 80's, when the problem of electron screening in nuclear reactions studied in laboratory was first analyzed [13,14]. The cross section determined by [5,10,11] and therefore the extrapolation reported in [3] and in [4] and the reaction

when the relative motion inside the Trojan-Horse nucleus is in s-wave, as is the case of the deuteron.

rates are likely to be affected by the enhancement due to atomic effects of nearly 10% [13] at 80 keV (corresponding to the lowest measured energy).

Thus the extrapolation was performed on data having a much larger value and a different low-energy behaviour with respect to the bare nucleus cross section, which is the relevant nuclear input parameter in astrophysical codes. In addition, since a large number of low-energy cross-section measurements have shown that the electron screening potential is much higher than what the adiabatic limit provides (for example, for the ^{3}He(d, p)^{4}He the electron screening potential turned out to be a factor two higher than the adiabatic limit [15]), an even higher overestimate of the ^{15}N(p, α)^{12}C S-factor inside the Gamow window is quite likely. As a consequence a further analysis of the ^{15}N(p, α)^{12}C low-energy data is needed with through both direct and indirect methods.

References

1. M. Lugaro *et al.*, Ap. J. **615**, 934 (2004).
2. A. Renda *et al.*, Mon. Not. R. Astron. Soc. **354**, 575 (2004).
3. C. Angulo *et al.*, Nucl. Phys. A **656**, 3 (1999).
4. G.R. Coughlan, W.A. Fowler, At. Data Nucl. Data Tables **40**, 283 (1988).
5. A. Redder *et al.*, Z. Phys. A **305**, 325 (1982).
6. F. Strieder *et al.*, Naturwissenschaften **88**, 461 (2001).
7. G. Baur, Phys. Lett. B **178**, 135 (1986).
8. C. Spitaleri *et al.*, Phys. Rev. C **69**, 055806 (2004).
9. C. Spitaleri *et al.*, Phys. Rev. C **63**, 055801 (2001).
10. A. Schardt *et al.*, Phys. Rev. **86**, 527 (1952).
11. J.L. Zyskind *et al.*, Nucl. Phys. A **320**, 404 (1979).
12. S. Typel *et al.*, Ann. Phys. (N.Y.) **305**, 228 (2003).
13. H.J. Assenbaum *et al.*, Z. Phys. A **327**, 461 (1987).
14. G. Blüge *et al.*, Z. Phys. A **333**, 219 (1989).
15. M. Aliotta *et al.*, Nucl. Phys. A **690**, 790 (2001).